Dynamically Reconfigurable Photonic Crystal Nanobeam Cavities

Ian W. Frank†, Parag B. Deotare†, Murray W. McCutcheon, Marko Lončar*
School of Engineering and Applied Sciences,
Harvard University, Cambridge, MA 02138
† These authors contributed equally to this work.
* e-mail: loncar@seas.harvard.edu

September 11, 2009

Abstract

Wavelength-scale, high Q-factor photonic crystal cavities [1, 2] have emerged as a platform of choice for on-chip manipulation of optical signals, with applications ranging from low-power optical signal processing [3] and cavity quantum electrodynamics [4, 5] to biochemical sensing. Many of these applications, however, are limited by the fabrication tolerances and the inability to precisely control the resonant wavelength of fabricated structures. Various techniques for post-fabrication wavelength trimming [6, 7] and dynamical wavelength control – using, for example, thermal effects [8, 9, 10], free carrier injection [11], low temperature gas condensation [12], and immersion in fluids [13] – have been explored. However, these methods are often limited by small tuning ranges, high power consumption, or the inability to tune continuously or reversibly. In this letter, by combining nano-electro-mechanical systems (NEMS) and nanophotonics, we demonstrate reconfigurable photonic crystal nanobeam cavities that can be continuously and dynamically tuned using electrostatic forces. A tuning of $\sim$ 10 nm has been demonstrated with less than 6 V of external bias and negligible steady-state power consumption.

Recently, it has been theoretically predicted [14, 15, 16] and experimentally verified [2, 17, 18, 19] that photonic crystal nanobeam cavities (PhCNB) can have ultra-high quality factors, on-par with those demonstrated in conventional photonic crystal cavities based on a two-dimensional lattice of holes. PhCNB cavities can be viewed as a doubly clamped nanobeam, the simplest NEMS device, perforated with a one-dimensional lattice of

holes, a textbook example of an optical grating. By introducing an appropriate chirp in the grating, ultra-high Q factors and small mode volume optical resonators can be realized [2]. When two PhCNB cavities are placed in each other's near field, as shown in Fig. 1, their resonant modes couple, resulting in two supermodes with resonant frequencies that are highly dependent on the spacing between the nanobeams [20]. This can be attributed to two major factors. First, the coupling between the two resonators increases with the reduction in the lateral separation between the nanobeams, which results in greater splitting between the two supermodes. At the same time, as the nanobeams are drawn closer together, the higher order effect of the coupling induced frequency shift [21] becomes significant (especially for separations < 100 nm) and red shifting of both of the supermodes occurs. The net effect of these two factors is that the even supermode experiences a considerable red shift as the separation is reduced, while the wavelength of the odd supermode stays relatively constant (the two effects cancel out) [20].

The strong dependence of the wavelength of the even supermode on the separation between two nanobeams renders coupled-PhCNB cavities highly suited for applications in motion and mass sensing. In addition, the strong optical fields that exist in the air region between the coupled-PhCNB cavities makes these devices excellent candidates for biochemical sensing applications. Finally, by simultaneously taking advantage of both the optical and mechanical degrees of freedom of such these cavities, a plethora of exciting optomechanical phenomena can be realized [18, 22].

In this work, we take advantage of the mechanical flexibility of coupled PhCNBs to realize reconfigurable optomechanical devices that can be electrostatically actuated [23]. By applying a potential difference directly across the nanobeams, an attractive electrostatic force can be induced between the two nanobeams, resulting in a decrease of the gap between the nanobeams, as can be seen in Fig. 1 b and c. This, in turn, results in the change of the resonant wavelength of the two supermodes. Self-consistent optical and mechanical finite-element simulations were used to model the deflection of the nanobeams due to the electrostatic forces, and its influence on the optical eigenfrequencies (Fig. 1c). Fig. 1d shows the dependence of the nanobeam separation (red curve) on the applied voltage, as well as the differential separation change for different bias voltages, in the case of a device with 77 nm initial separation between nanobeams. It can be seen that nanobeam separation, measured at the middle of the nanobeams, can be reduced to 50nm with ≈ 5 V of external bias. Moreover, the change in the separation per unit of applied voltage strongly depends on the applied bias, and is on the order of 25 nm/V for $V \approx 5$ V. The influence of the

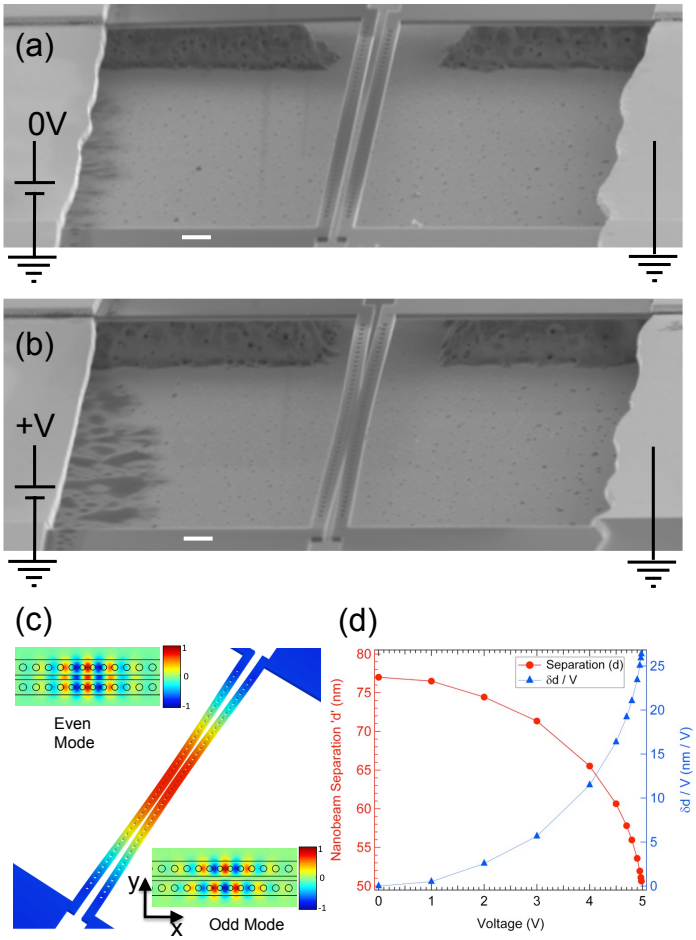

Figure 1: **Coupled photonic crystal nanobeam cavities.** **a**, SEM image of a representative fabricated structure. The suspended silicon is in contact with gold electrodes seen at the edge of the image and is supported by islands of SiO_2 (scalebar = 1 μm). **b**, SEM image showing the deflection of the nanobeams due to electrostatic actuation. **c**, Finite element simulations showing nanobeams deflected due to an applied potential. The insets depict the E_y component of the optical supermodes of the coupled cavities. **d**, Simulation data: the red curve shows the lateral separation of a pair of nanobeams, measured at the center of the structure, as a potential is applied across them, while the blue curve shows the sensitivity of the deflection with respect to the applied voltage.

electrostatically-controlled nanobeam separation on the resonances of two supermodes is shown in Fig. 2a. We found that, in our system, the even supermode red shifts while the odd supermode experiences very little dispersion (remaims effectively stationary). This is in good agreement with our previous results [20], where the dependence of the supermode eigenfrequencies on lithographically-defined separations (static tuning) was studied.

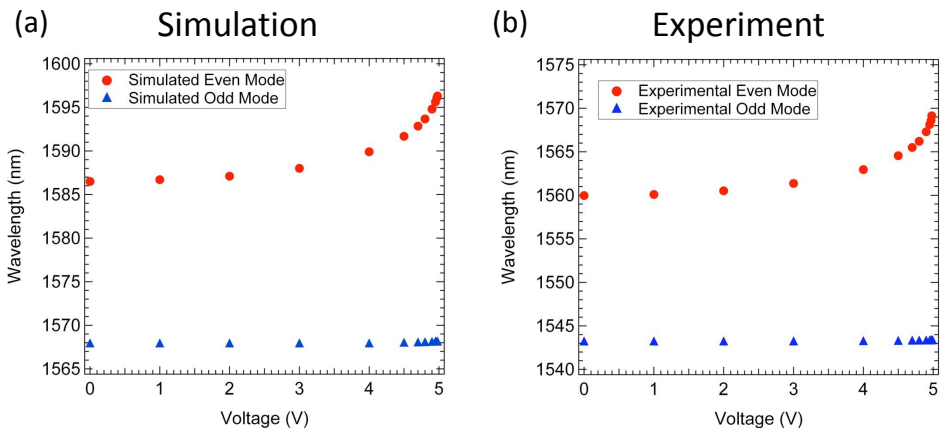

Figure 2: **Electrostatic tuning of a coupled photonic crystal nanobeam cavity. a**, Finite element simulations showing the dependence of the even (shown in red) and odd (blue) supermode resonance on the applied bias voltage. **b**, Experimental data showing the measured resonances for even and odd supermodes. The trend seen in the experimental data matches well with the simulated results. The slight discrepancy in the absolute value of resonant wavelength can be attributed to uncertainty in the thickness and refractive index of the device layer of the SOI wafer, as well as the amount of tensile stress in the nanobeams.

Encouraged by these results, we fabricated our opto-mechanical devices using similar techniques to those reported in our previous work [20]. The principal difference here is that the two PhCNBs are electrically isolated. Furthermore, in order to make electrical contact to each nanobeam, Au contact pads were lithographically patterned onto the substrate (see Methods section). An electron micrograph of a fabricated structure is shown in Fig. 1a. The optical characterization of the fabricated structures was performed using a resonant scattering setup [24, 25] (see Methods section). A normally incident tunable laser-beam was focused down onto the cavities and

the resonantly back-scattered signal was analyzed after cross-polarizing it with respect to the incoming wave. Fig. 2b shows the experimental results for the nanobeam cavities, illustrating the dependence of the even and odd supermode eigenfrequencies on the applied bias voltage. Very good agreement with numerical modeling can be observed. The experimentally measured resonant wavelengths were within 2% of the simulated ones, and the tuning trend matched very well with the theoretical predictions. The slight discrepancy can be attributed to several effects, including the uncertainty in the refractive index of the doped silicon device layer, variations in the layer thickness, and uncertainty in the amount of tensile stress in the device layer of the SOI ($\pm$25 MPa, according to SOITEC). The optical Q factor of the modes was determined by a Fano fit [26] (see Methods section) to the scattered waveform. The Q factor of the even mode was around $13,000$ while that of the odd mode was around $50,000$. In this work, we intentionally designed and fabricated cavities with a lower Q in order to facilitate experimental characterization via the resonant scattering approach. In our previous work, we demonstrated that coupled PhCNB cavities can have Q factors in the $10^5 - 10^6$ range [20]. It is important to emphasize that the Q factors did not change observably across the whole tuning range. This is in stark contrast to tuning via free-carrier injection, which results in significant reduction in the cavity Q factor due to free-carrier absorption.

In our best devices, we were able to shift the resonant wavelength of the even supermode up to 9.6 nm when less than 6 V of external bias voltage was applied (Fig. 3a). This wide tuning range is nearly 80 times larger than the linewidth of the cavity resonance in the present design, and this ratio can be further improved by increasing the Q factor of the fabricated cavities. Fig. 3a also shows the sensitivity plot for the measured cavity, defined as the change in the resonant wavelength for a given voltage change. It can be seen that by operating the system at $\sim$ 6 V bias voltage, sensitivities as large as 50 nm/V can be measured. In other words, in this regime, as little as a 5 mV change in the bias voltage would result in a wavelength change larger than the full-width at half-maximum ($FWHM \sim 0.1$ nm) of the cavity resonance. This is advantageous for the realization of applications such as low-power optical switches and reconfigurable filters/routers. The high sensitivity of our devices can be attributed to two factors: (i) the dependence of the wavelength shift on the change in separation is intrinsically nonlinear [20], and much larger shifts are obtained as the nanobeam separation becomes smaller, as in the case of higher voltages; (ii) the electrostatic force experienced by the nanobeams is quadratic with the applied bias voltage as well as inversely-proportional to the nanobeam separation. It is

important to emphasize that in the steady state, when the system is reconfigured and the nanobeams are deflected to their final position, our system is not drawing any power from the bias source (beyond what might result from leakage currents through the thick SiO_2 layer underneath the Si device layer). This is of great practical interest for the realization of reconfigurable devices and systems, as mentioned above. The high sensitivities and high Q factors of coupled-PhCNB cavities are also suitable for precision motion measurements in NEMS devices, since a strong modulation of the optical signal can be achieved, even for tiny displacements of the nanobeams. Finally, coupled-PhCNB cavities hold great promise for exciting applications involving the adiabatic wavelength conversion of light trapped in optical cavities [27, 28, 11] through mechanical motion.

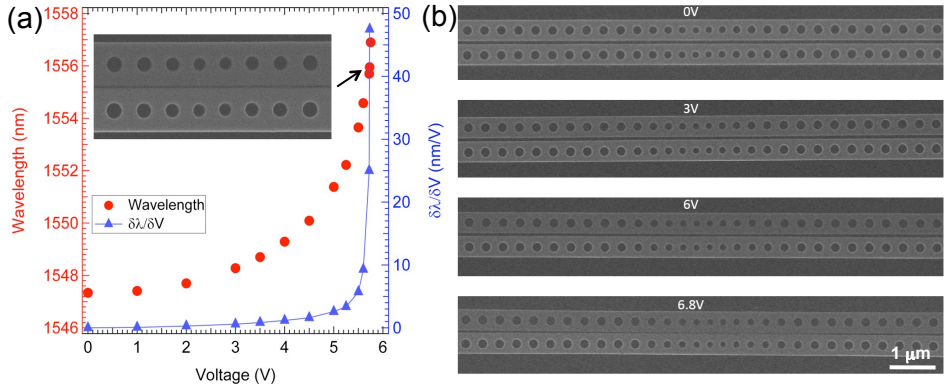

Figure 3: **Sensitivity of the coupled-cavity resonance and visualization of nanobeams deflection due to the applied voltage**. **a**, Experimental results showing the resonant wavelength of the even supermode as the bias voltage is stepped up to 6 V (red curve). Tuning up to 9.6nm is obtained in this cavity. The blue curve shows the sensitivity of the same cavity resonance to the applied voltage. A high sensitivity of 50 nm/V is obtained when cavity is operated around 6 V bias voltage. The results are obtained for a cavity with initial (V=0) nanobeam separation of $\sim$ 70 nm. **b**, Scanning electron microscopy images showing deflection of a pair of nanobeams under different bias voltages. The lower nanobeam remains grounded, while the potential on the upper nanobeam is increased as indicated.

By utilizing an electrical feed-through port on a scanning electron microscope (SEM), we were able to observe the real-time deflection of the

devices due to the applied bias voltage. Fig. 3b shows SEM images of the two nanobeams with increasing voltages applied across them. The images are shown for nanobeams with a large initial separation ($V_{bias} = 0$) of 100 nm, in order to render the motion of the nanobeams more distinctly. The bending of the nanobeams at the center of the structure can easily be observed, and matches well with our theoretical predictions (Fig. 1c). After the pull-in voltage [29] is exceeded, the two beams can become permanently stuck together due to van der Waals interactions. Finally, we note that the difference in steady-state performance of our structures when operated in vacuum (inside the SEM chamber) and in the atmospheric conditions (resonant scattering setup) is negligible, as in either case the structure is operated well below the breakdown voltage.

The current limitation to the tuning method employed here is the RC (resistance $\times$ capacitance) time constant of the system. The resistance offered by the silicon nanobeams is on the order of $10^{11}\,\Omega$, resulting in time constants in the tens of seconds, despite the small capacitance of the structure. This could be readily improved by doping the silicon, albeit at the expense of the cavity Q factors (due to increased material loss). The performance of the system could be further improved by utilizing alternative actuation methods [30] that do not depend on the RC time constant of the coupled nanobeams. In that case, the response time would be limited by the mechanical response, which is on the order of ~ 100 ns in the present design.

In summary, we have demonstrated reconfigurable optical filters that can be dynamically and reversibly tuned using electrostatic forces over ≈ 10 nm wavelength range when less than 6 V of external bias voltage is applied to the structure. This work will serve as a basis for exciting applications ranging from ultra-sensitive motion detection to electrically actuated switching in optical circuits. The tuning method is stable and remarkably reproducible, provided that the voltage is not raised beyond the point of pull-in. By allowing precision wavelength trimming of devices, this method also provides higher tolerances for fabrication errors, enabling diverse applications in optomechanics, cavity quantum electrodynamics, and optical signal processing.

1 Acknowledgements

This work is supported in part by NSF CAREER grant. Device fabrication was performed at the Center for Nanoscale Systems at Harvard. The authors would like to thank CNS Staff members David Lange and Steven Paolini for

their assistance. The authors would also like to thank Prof. Ming Wu for helpful discussions. M.W.M. would like to thank NSERC (Canada) for its support and I.W.F. thanks the NSF GRFP.

References

[1] Song, B., Noda, S., Asano, T. & Akahane, Y. Ultra-high-q photonic double-heterostructure nanocavity. *Nature Mat.* **4**, 207–210 (2005).

[2] Deotare, P. B., McCutcheon, M. W., Frank, I. W., Khan, M. & Loncar, M. High quality factor photonic crystal nanobeam cavities. *Appl. Phys. Lett.* **94**, 121106 (2009).

[3] Tanabe, T., Notomi, M., Mitsugi, S., Shinya, A. & Kuramochi, E. All-optical switches on a silicon chip realized using photonic crystal nanocavities. *Appl. Phys. Lett.* **87**, 151112 (2005).

[4] Hennessy, K. *et al.* Quantum nature of a strongly coupled single quantum dot-cavity system. *Nature* **445**, 896–899 (2007).

[5] Englund, D. *et al.* Controlling cavity reflectivity with a single quantum dot. *Nature* **450**, 857–861 (2007).

[6] Yang, X., Chen, C. J., Husko, C. A. & Wong, C. W. Digital resonance tuning of high-Q/Vm silicon photonic crystal nanocavities by atomic layer deposition. *Appl. Phys. Lett.* **91**, 161115 (2007).

[7] Faraon, A. *et al.* Local tuning of photonic crystal cavities using chalcogenide glasses. *Appl. Phys. Lett.* **92**, 043123 (2008).

[8] Pan, J. *et al.* Aligning microcavity resonances in silicon photonic-crystal slabs using laser-pumped thermal tuning. *Appl. Phys. Lett.* **92**, 103114 (2008).

[9] Marki, I. *et al.* Optically tunable microcavity in a planar photonic crystal silicon waveguide buried in oxide. *Opt. Lett.* **31**, 513–515 (2006).

[10] Fushman, I. *et al.* Ultrafast nonlinear optical tuning of photonic crystal cavities. *Appl. Phys. Lett.* **90**, 091118 (2007).

[11] McCutcheon, M. W., Pattantyus-Abraham, A. G., Rieger, G. W. & Young, J. F. Emission spectrum of electromagnetic energy stored in a dynamically perturbed optical microcavity. *Opt. Express* **15**, 11472–11480 (2007).

[12] Mosor, S. *et al.* Scanning a photonic crystal slab nanocavity by condensation of xenon. *Appl. Phys. Lett.* **87**, 141105 (2005).

[13] Maune, B. *et al.* Liquid-crystal electric tuning of a photonic crystal laser. *Appl. Phys. Lett.* **85**, 360–362 (2004).

[14] Sauvan, C., Lecamp, G., Lalanne, P. & Hugonin, J. Modal-reflectivity enhancement by geometry tuning in photonic crystal microcavities. *Opt. Express* **13**, 245–255 (2005).

[15] McCutcheon, M. W. & Loncar, M. Design of a silicon nitride photonic crystal nanocavity with a quality factor of one million for coupling to a diamond nanocrystal. *Opt. Express* **16**, 19136–19145 (2008).

[16] Notomi, M., Kuramochi, E. & Taniyama, H. Ultrahigh-q nanocavity with 1d photonic gap. *Opt. Express* **16**, 11095–11102 (2008).

[17] Zain, A. R. M., Johnson, N. P., Sorel, M. & la Rue, R. M. D. Ultra high quality factor one dimensional photonic crystal/photonic wire micro-cavities in silicon-on-insulator (soi). *Opt. Express* **16**, 12084–12089 (2008).

[18] Eichenfield, M., Camacho, R., Chan, J., Vahala, K. J. & Painter, O. A picogram- and nanometre-scale photonic-crystal optomechanical cavity. *Nature* **459**, 550–U79 (2009).

[19] Velha, P. *et al.* Ultra-high q/v fabry-perot microcavity on soi substrate. *Opt. Express* **15**, 16090–16096 (2007).

[20] Deotare, P. B., McCutcheon, M. W., Frank, I. W., Khan, M. & Loncar, M. Coupled photonic crystal nanobeam cavities. *Appl. Phys. Lett.* **95**, 031102 (2009).

[21] Popovic, M., Manolatou, C. & Watts, M. Coupling-induced resonance frequency shifts in coupled dielectric multi-cavity filters. *Opt. Express* **14**, 1208–1222 (2006).

[22] Eichenfield, M., Chan, J., Camacho, R., Vahala, K. J. & Painter, O. Optomechanical crystals **arXiv:0906.1236** (2009).

[23] Lee, M. & Wu, M. Tunable coupling regimes of silicon microdisk resonators using mems actuators. *Opt. Express* **14**, 4703–4712 (2006).

[24] McCutcheon, M. *et al.* Resonant scattering and second-harmonic spectroscopy of planar photonic crystal microcavities. *Appl. Phys. Lett.* **87**, 221110 (2005).

[25] Altug, H. & Vuckovic, J. Polarization control and sensing with two-dimensional coupled photonic crystal microcavity arrays. *Opt. Lett.* **30**, 982–984 (2005).

[26] Galli, M. *et al.* Light scattering and fano resonances in high-q photonic crystal nanocavities. *Appl. Phys. Lett.* **94**, 071101 (2009).

[27] Preble, S. F., Xu, Q. & Lipson, M. Changing the colour of light in a silicon resonator. *Nature Photon.* **1**, 293–296 (2007).

[28] Tanabe, T., Notomi, M., Taniyama, H. & Kuramochi, E. Dynamic release of trapped light from an ultrahigh-q nanocavity via adiabatic frequency tuning. *Phys. Rev. Lett.* **102**, 043907 (2009).

[29] Liu, C. *Foundations of MEMS* (Prentice Hall, Upper Saddle River, 2005).

[30] Unterreithmeier, Q. P., Weig, E. M. & Kotthaus, J. P. Universal transduction scheme for nanomechanical systems based on dielectric forces. *Nature* **458**, 1001–1004 (2009).

Methods

Device Fabrication

The devices were fabricated on a SOI substrate with a 220 nm device layer using a standard electron beam lithography followed by an ICP reactive ion etching in a SF_6-C_4F_8 plasma. The nanobeams were laterally separated by a distance as small as 50 nm. Photolithography was used to pattern Cr/Au electrodes for electrical contact with each isolated beam. A thin layer of Cr is used as an adhesive layer for the Au electrodes. A hydrofluoric acid vapor etch was performed to release the structures. Finally, contact was made to the gold electrodes by ultrasonic wirebonding to a ceramic chip-carrier.

Device Characterization

The devices were characterized using a resonant scattering setup. A CW beam was passed through a polarizer and rotated by 45° using a half-wave plate before entering the objective lens. The resonantly scattered signal was collected by the same objective lens, split using a non-polarizing beam-splitter, analyzed using a linear polarizer which was cross polarized with respect to the input beam, and finally detected using an InGaAs detector. This method enhances the ratio between the resonantly scattered signal and the nonresonant background reflection, without loading the cavity. Due to the inherent symmetry of the excitation field, the resonant modes of the two cavities are more naturally driven in phase, which facilitates the measurement of the even supermodes of the coupled cavities. However, by taking advantage of a gradient in the excitation fields (by offsetting the excitation beam), we were also able to probe the odd supermodes.

To obtain the quality factor of the cavity, the scattered signal from the cavity was first normalized to the background taken away from the cavity but along the beam. The data were then fitted with the Fano lineshape

$$F(\omega) = A_0 + F_0 \frac{[q + 2(\omega - \omega_0)/\Gamma]^2}{1 + [2(\omega - \omega_0)/\Gamma]^2} \tag{1}$$

where ω is the frequency of the cavity mode, Γ is the FWHM and A_0 and F_0 are constants to obtain the Quality Factor (Q) [26].